

Impact of non-standard neutrino-electron interactions on Big Bang Nucleosynthesis

Stefano Gariazzo^{a,b}, Jaume Moncho^{b,c}, Sergio Pastor^b, Ofelia Pisanti^{d,e}

^a*University of Turin, Physics department and INFN, Sezione di Torino, Via P. Giuria 1, I-10125 Torino, Italy*

^b*Instituto de Física Corpuscular (IFIC), CSIC-Universitat de València*

Parc Científic UV, C/ Catedrático José Beltrán, 2, E-46980 Paterna (València), Spain

^c*Departament de Física Teòrica, Universitat de València, C/ Dr. Moliner, 50, 46100 Burjassot (València), Spain*

^d*Dipartimento di Fisica “Ettore Pancini”, Università degli studi di Napoli “Federico II”, Complesso Univ. di Monte S. Angelo, I-80126 Napoli, Italy*

^e*INFN - Sezione di Napoli, Complesso Univ. di Monte S. Angelo, I-80126 Napoli, Italy*

Abstract

Neutrino non-standard interactions (NSI) with electrons, predicted in many extended theoretical models of particle physics, are known to alter the picture of neutrino decoupling from the cosmic plasma. We update previous analyses of neutrino decoupling in presence of NSI with electrons, extending the parameter space in order to provide, for the first time, a full study of their effect on the production of light elements during Big Bang Nucleosynthesis (BBN). We compare the BBN bounds on non-universal and flavour-changing NSI parameters with the constraints from terrestrial experiments. Our results show that the limits from BBN are significantly less stringent than the experimental bounds, but they are complementary and can provide a test of neutrino physics at different temperature scales and epochs.

Keywords: neutrino interactions, non-standard neutrino interactions, cosmology, neutrino oscillations.

1. Introduction

Present data from solar, atmospheric, reactor and accelerator neutrino experiments are well described by the existence of flavour oscillations in the framework of three-neutrino mixing (see e.g. [1]). This experimental evidence for non-zero neutrino masses and mixing calls for new physics beyond the Standard Model (SM) of fundamental particles and forces. The presence of non-standard interactions (NSI) of neutrinos with other fermions and among themselves is predicted by a variety of extended theoretical models. Such new interactions can leave an imprint on different observations and experiments, including the pattern of neutrino oscillations in matter, neutrino scattering at production and detection, and neutrino interaction measurements. By analysing a combination of all available data, there is currently no evidence in favour of NSI, and bounds have been derived, as reviewed e.g. in [2], but their existence would have implications in cosmological and astrophysical scenarios.

In the early universe, neutrinos are kept in equilibrium by weak interactions, which become ineffective at a temperature of $\mathcal{O}(\text{MeV})$. At this point, neutrinos decouple and constitute the cosmological neutrino background. The neutrino decoupling process is very well understood, see e.g. [3, 4, 5], where the effective number of relativistic species has been calculated to be $N_{\text{eff}} = 3.044$. Such number is defined in order to quantify the amount of energy density (ρ_{rad}) carried by relativistic, neutrino-like relics with respect to the photon one (ρ_{γ}) [6]:

$$\rho_{\text{rad}} = \rho_{\gamma} \left(1 + \frac{7}{8} \left(\frac{4}{11} \right)^{4/3} N_{\text{eff}} \right). \quad (1)$$

Email addresses: gariazzo@ific.uv.es (Stefano Gariazzo), jaumon@ific.uv.es (Jaume Moncho), pastor@ific.uv.es (Sergio Pastor), pisanti@na.infn.it (Ofelia Pisanti)

Measurements of the cosmological microwave background (CMB) anisotropies by Planck, combined with other cosmological data, constrain $N_{\text{eff}} = 2.99_{-0.33}^{+0.34}$ at 95% C.L. [7]. Such value severely restricts the possible existence of additional relativistic particles.

The presence of NSI could modify the decoupling process of cosmological neutrinos, as noted already in [8, 9]. In particular, non-standard interactions with electrons, the only charged leptons that are still abundant at MeV cosmological temperatures, would modify the thermal contact of neutrinos with the electromagnetic plasma and change their momentum spectra, leading to a different value of N_{eff} . Earlier analyses of the effect of NSI on N_{eff} include [10, 11], but these works only considered some particular choices of the NSI parameters. More recently, the effect of NSI on neutrino decoupling has been quantified in [12], where a complete numerical treatment of NSI in this context has been developed.

In contrast to the study of neutrino decoupling, a full analysis of NSI effects on Big Bang Nucleosynthesis (BBN) has not been performed yet. A partial study, involving NSI interactions of neutrinos with quarks, was published recently in [13]. In this case, the weak interaction processes that govern the equilibrium of protons and neutrons at the beginning of BBN, the so-called weak rates, are modified. This implies that the produced amount of light elements, and in particular helium-4, are modified by the initial ratio of neutrons with respect to protons.

Instead, if one considers NSI between neutrinos and electrons alone, there is no direct effect on the weak rates but the presence of NSI modifies the total energy density of radiation in the universe and leads to distortions in the momentum distribution function of electron neutrinos. Thus, the effect on the light element abundances is different but it can still be appreciable. This is the objective of the present paper, where we also compare the results with current observations of the primordial abundances.

2. Neutrino non-standard interactions with electrons

Non-standard neutrino interactions arise in a broad class of extensions of the SM that generate neutrino masses and mixing. At energies well below the electroweak scale, such effects can be described in terms of effective four-fermion operators that modify the interactions between neutrinos and matter fields.

For the range of cosmological temperatures during neutrino decoupling, the only abundant charged leptons in the primordial plasma were electrons and positrons. Consequently, we restrict our analysis to neutral-current NSI of neutrinos with electrons. Taking this into account, the effective Lagrangian density describing neutrino–electron interactions can be written as

$$\mathcal{L} = \mathcal{L}_{\text{SM}} + \mathcal{L}_{\text{NC-NSI}e}, \quad (2)$$

where the SM contribution reads

$$\mathcal{L}_{\text{SM}} = -2\sqrt{2}G_F \left[(\bar{\nu}_e \gamma^\mu P_L e) (\bar{e} \gamma_\mu P_L \nu_e) + g_X (\bar{\nu}_\alpha \gamma^\mu P_L \nu_\alpha) (\bar{e} \gamma_\mu P_X e) \right] \quad (3)$$

Here, G_F denotes the Fermi constant and $X = L, R$ is the chirality, so that $P_{R,L} = (1 \pm \gamma_5)/2$ are the usual left- or right-handed chirality projection operators, and $g_L = \sin^2 \theta_W - 1/2$, $g_R = \sin^2 \theta_W$ are the SM neutral-current couplings, with θ_W being the weak mixing angle. The NSI contribution is described by

$$\mathcal{L}_{\text{NC-NSI}e} = -2\sqrt{2}G_F \varepsilon_{\alpha\beta}^X (\bar{\nu}_\alpha \gamma^\mu P_L \nu_\beta) (\bar{e} \gamma_\mu P_X e), \quad (4)$$

where the dimensionless parameters $\varepsilon_{\alpha\beta}^X$ quantify the strength of the non-standard interactions between neutrinos of flavours α and β and electrons. The sums over flavours α, β and chiralities X are implicit in both equations.

We talk about *flavour-changing* NSI when $\varepsilon_{\alpha\beta} \neq 0$ for $\alpha \neq \beta$, since they correspond to lepton flavour non-conserving interactions. On the other hand, if $\varepsilon_{\alpha\alpha} - \varepsilon_{\beta\beta} \neq 0$, we refer to them as *non-universal* NSI, as they break lepton flavour universality.

Bounds on neutrino NSI with electrons can be derived from a combination of data from neutrino oscillation experiments, neutrino–electron scattering measurements, and precision constraints from LEP. Oscillation and scattering experiments constrain different combinations of NSI parameters through their impact on neutrino propagation and detection processes, respectively.

Table 1: Current bounds on non-universal and flavour-changing NSI with electrons at 90% C.L. for 1 degree of freedom. Adapted from [2, 15]

Parameter and 90% C.L. range	Origin
$-0.021 < \varepsilon_{ee}^L < 0.052$	Neutrino oscillations [16]
$-0.07 < \varepsilon_{ee}^R < 0.08$	Scattering data[17]
$-0.23 < \varepsilon_{ee}^R < 0.07$	Neutrino oscillations [18]
$-0.03 < \varepsilon_{\mu\mu}^{L,R} < 0.03$	Scattering and accelerator data [19]
$-0.12 < \varepsilon_{\tau\tau}^L < 0.06$	Neutrino oscillations [16]
$-0.98 < \varepsilon_{\tau\tau}^R < 0.23$	Neutrino oscillations [16, 20]
$-0.25 < \varepsilon_{\tau\tau}^R < 0.43$	Scattering and accelerator data [16]
$-0.13 < \varepsilon_{e\mu}^{L,R} < 0.13$	Scattering and accelerator data [19]
$-0.33 < \varepsilon_{e\tau}^L < 0.33$	Scattering and accelerator data [19]
$-0.28 < \varepsilon_{e\tau}^R < -0.05$ & $0.05 < \varepsilon_{e\tau}^R < 0.28$	Scattering and accelerator data [19]
$-0.19 < \varepsilon_{e\tau}^R < 0.19$	Scattering data[17]
$-0.10 < \varepsilon_{\mu\tau}^{L,R} < 0.10$	Scattering and accelerator data [19]

In Table 1 we present a compilation of bounds on neutrino non-standard interactions with electrons, obtained under the assumption that only one NSI parameter is non-zero at a time. If correlations between different parameters are taken into account, the allowed parameter space becomes larger, because of degeneracies and cancellations that may appear among different NSI coefficients. In order to obtain more robust bounds, one possibility is to vary several NSI parameters at the same time, and then to marginalise over some of them in order to present 1-dimensional constraints. We note that more recent analyses of NSI constraints have appeared in the literature, based on global fits that adopt a marginalisation procedure and employ alternative parameterisations of the interaction structure (see e.g. [14]). The resulting bounds are therefore not directly comparable to those reported here. The limits summarised in our work are chosen for consistency with the one-parameter scans performed in our cosmological analysis and to facilitate a transparent comparison with previous studies.

3. Impact of non-standard interactions on neutrino decoupling

In order to consistently account for neutrino flavour oscillations, spectral distortions, and non-standard interactions during the decoupling process, we adopt the density matrix formalism, where the density matrix is defined as

$$\varrho(t, p) = \begin{pmatrix} \varrho_{ee} & \varrho_{e\mu} & \varrho_{e\tau} \\ \varrho_{\mu e} & \varrho_{\mu\mu} & \varrho_{\mu\tau} \\ \varrho_{\tau e} & \varrho_{\tau\mu} & \varrho_{\tau\tau} \end{pmatrix} = \begin{pmatrix} f_{\nu_e} & \varrho_{e\mu} & \varrho_{e\tau} \\ \varrho_{\mu e} & f_{\nu_\mu} & \varrho_{\mu\tau} \\ \varrho_{\tau e} & \varrho_{\tau\mu} & f_{\nu_\tau} \end{pmatrix}. \quad (5)$$

The diagonal elements are the momentum distribution functions of the different neutrino flavours, and the off-diagonal elements are non-zero in the presence of mixing and implement the coherence of the system. Using the comoving variables (see e.g. [5, 21]) $x = m_e a$, $y = pa$, $z = T_\gamma a$; where m_e is the electron mass, p the neutrino momentum, T_γ the photon temperature and a the cosmological scale factor, the evolution of ϱ is given by the Boltzmann equation, written as

$$\frac{d\varrho(y)}{dx} = \sqrt{\frac{3m_{Pl}^2}{8\pi\rho}} \left\{ -i \frac{x^2}{m_e^3} \left[\frac{M_F}{2y} - \frac{2\sqrt{2}G_F y m_e^6}{x^6} \left(\frac{\mathbb{E}_\ell + \mathbb{P}_\ell}{m_W^2} + \frac{4}{3} \frac{\mathbb{E}_\nu}{m_Z^2} \right), \varrho(y) \right] + \frac{m_e^3}{x^4} \mathcal{I}(\varrho) \right\}, \quad (6)$$

where m_W and m_Z are the masses of the gauge bosons W^\pm and Z , ρ is the total energy density of the universe, \mathbb{E}_ℓ , \mathbb{P}_ℓ and \mathbb{E}_ν are matrices that represent the energy density and pressure of charged leptons and neutrinos and $\mathcal{I}(\varrho)$ encodes all the scattering/annihilations of the system involving electrons and positrons and also neutrino-neutrino interactions (for details, see [21]). The square brackets denote the commutator. In addition, \mathbb{M}_F is the rotated neutrino mass matrix in the flavour basis,

$$\mathbb{M}_F = U \begin{pmatrix} 0 & 0 & 0 \\ 0 & \Delta m_{21}^2 & 0 \\ 0 & 0 & \Delta m_{31}^2 \end{pmatrix} U^\dagger, \quad (7)$$

where Δm_{21}^2 and Δm_{31}^2 are the mass-squared differences between neutrino mass eigenstates, and U is the PMNS (Pontecorvo-Maki-Nakagawa-Sakata) mixing matrix.

The key point for assessing the impact of NSI on N_{eff} is that the collisional integrals $\mathcal{I}(\varrho)$ depend on the couplings that appear in the neutrino-electron scattering amplitudes. In the Standard Model, these couplings are encoded in the matrices (in flavour space)

$$G_L^{\text{SM}} = \text{diag}(\tilde{g}_L, g_L, g_L), \quad G_R^{\text{SM}} = \text{diag}(g_R, g_R, g_R), \quad (8)$$

where $\tilde{g}_L = \sin^2 \theta_W + 1/2$ takes into account the charged-current contribution in the case of electron neutrinos. When NSI with electrons are present, these matrices are modified and they read

$$G_L = \begin{pmatrix} \tilde{g}_L + \varepsilon_{ee}^L & \varepsilon_{e\mu}^L & \varepsilon_{e\tau}^L \\ \varepsilon_{\mu e}^L & g_L + \varepsilon_{\mu\mu}^L & \varepsilon_{\mu\tau}^L \\ \varepsilon_{\tau e}^L & \varepsilon_{\tau\mu}^L & g_L + \varepsilon_{\tau\tau}^L \end{pmatrix}, \quad G_R = \begin{pmatrix} g_R + \varepsilon_{ee}^R & \varepsilon_{e\mu}^R & \varepsilon_{e\tau}^R \\ \varepsilon_{\mu e}^R & g_R + \varepsilon_{\mu\mu}^R & \varepsilon_{\mu\tau}^R \\ \varepsilon_{\tau e}^R & \varepsilon_{\tau\mu}^R & g_R + \varepsilon_{\tau\tau}^R \end{pmatrix}. \quad (9)$$

Since the collisional integrals $\mathcal{I}(\varrho)$ involve products of the coupling matrices — one can find the full expressions in [5] — the presence of NSI leads to shifts in the corresponding Standard Model coefficients. In particular, the effective couplings entering the scattering terms are modified as follows:

$$g_L^2 \longrightarrow (g_L + \varepsilon_{\alpha\alpha}^L)^2 + \sum_{\beta \neq \alpha} |\varepsilon_{\alpha\beta}^L|^2, \quad (10)$$

$$g_R^2 \longrightarrow (g_R + \varepsilon_{\alpha\alpha}^R)^2 + \sum_{\beta \neq \alpha} |\varepsilon_{\alpha\beta}^R|^2, \quad (11)$$

$$g_L g_R \longrightarrow (g_L + \varepsilon_{\alpha\alpha}^L) (g_R + \varepsilon_{\alpha\alpha}^R) + \sum_{\beta \neq \alpha} |\varepsilon_{\alpha\beta}^L| |\varepsilon_{\alpha\beta}^R|. \quad (12)$$

These shifts modify the rate of neutrino interactions with the e^\pm plasma, hence affecting the dynamics of the decoupling process. Consequently, both the decoupling temperature and N_{eff} become sensitive to the NSI parameters $\varepsilon_{\alpha\beta}^{L,R}$.

Moreover, NSI also affect the matter-induced potentials responsible for flavour oscillations, and these modifications must be properly included in the evolution equation of the neutrino density matrix, specifically in the terms \mathbb{E}_ℓ and \mathbb{P}_ℓ of equation (6). These contributions can be encoded in the matrix

$$\mathbb{E}_e^{\text{NSI}} = \begin{pmatrix} 1 + \varepsilon_{ee}^V & \varepsilon_{e\mu}^V & \varepsilon_{e\tau}^V \\ \varepsilon_{\mu e}^V & \varepsilon_{\mu\mu}^V & \varepsilon_{\mu\tau}^V \\ \varepsilon_{\tau e}^V & \varepsilon_{\tau\mu}^V & \varepsilon_{\tau\tau}^V \end{pmatrix}, \quad (13)$$

so that the energy density and pressure contributions from the charged leptons read

$$\mathbb{E}_\ell = \rho_e \mathbb{E}_e^{\text{NSI}}, \quad \mathbb{P}_\ell = P_e \mathbb{E}_e^{\text{NSI}}, \quad (14)$$

where ρ_e and P_e are the electron energy density and pressure. These expressions contain the standard contribution (the unit term in the first element of $\mathbb{E}_e^{\text{NSI}}$) and NSI corrections that depend on both the left-

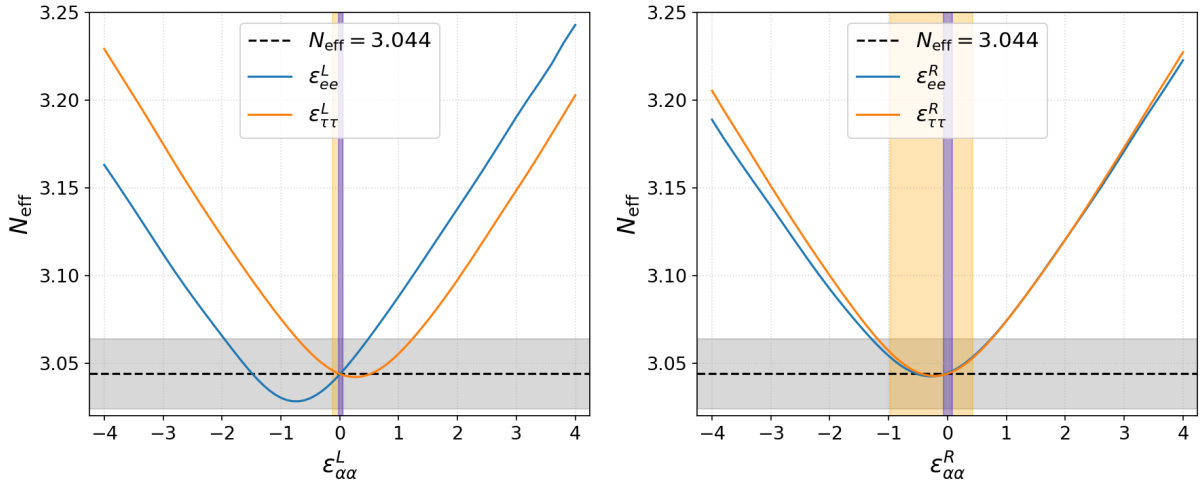


Figure 1: Values of N_{eff} as a function of non-universal NSI parameters, $\varepsilon_{\alpha\alpha}^L$ in the left panel and $\varepsilon_{\alpha\alpha}^R$ in the right panel, for $\alpha = \{e, \tau\}$. The dashed line corresponds to the standard prediction $N_{\text{eff}} = 3.044$, and the shaded region corresponds to ± 0.02 , which is the expected 1σ uncertainty from future cosmological observations [22]. The shaded vertical bands correspond to the 90% C.L. bounds shown in Table 1, in orange for the $\tau\tau$ coupling and in blue for the ee ones.

and right-handed couplings. Here, we have introduced the dimensionless parameter $\varepsilon_{\alpha\beta}^V \equiv \varepsilon_{\alpha\beta}^R + \varepsilon_{\alpha\beta}^L$, that is the vectorial coupling.

In order to include the full set of relevant effects in the determination of N_{eff} , we perform a complete numerical computation using the publicly available code **FortEPiano**¹ (Fortran-Evolved Primordial Neutrino Oscillations) [5, 21]. The numerical setup is chosen to ensure high precision, obtaining N_{eff} with a numerical error below 5×10^{-4} in the standard scenario, a level of precision sufficient to probe the small effects introduced by non-standard interactions. To reach this accuracy, the absolute and relative tolerances for the differential equation solver are set to 10^{-6} . The neutrino momentum integration is performed using Gauss-Laguerre quadrature with $N_y = 50$ momentum bins and a maximum comoving momentum $y_{\text{max}} = 20$. The initial conditions are set at $x_{\text{in}} = 0.01$, corresponding to a temperature much higher than the decoupling scale.

The results presented in this work for N_{eff} are analogous to those reported in Ref. [12]. Here, we extend that analysis by exploring a wider region of the NSI parameter space, in order to have an improved picture of the effects on BBN. Although a large part of this region is already disfavoured by terrestrial experiments, this will allow us to assess the sensitivity of neutrino decoupling and Big Bang Nucleosynthesis predictions to non-standard interactions in a complementary way and to identify the regions compatible with current cosmological observables. In addition, we do not consider the NSI parameters involving muon neutrinos because of the more stringent bounds from terrestrial experiments, see Table 1.

In Fig. 1, we show the values of N_{eff} as a function of $\varepsilon_{\alpha\alpha}^L$ (left panel) and $\varepsilon_{\alpha\alpha}^R$ (right panel), for $\alpha = \{e, \tau\}$, varying one parameter at a time while keeping all others fixed to zero. For the case of ε_{ee}^L , the minimum of N_{eff} occurs at $\varepsilon_{ee}^L = -\tilde{g}_L = -\frac{1}{2} - \sin^2 \theta_W$, as expected from the shift in the coupling structure. In this configuration, the effective left-handed coupling to electrons vanishes, suppressing neutrino-electron interactions and leading to an earlier decoupling. Similarly, for $\varepsilon_{\tau\tau}^L$, the minimum is found at $\varepsilon_{\tau\tau}^L = -g_L = \frac{1}{2} - \sin^2 \theta_W$, where the coupling to tau neutrinos cancels. An analogous argument applies to the right-handed couplings. The minimum of N_{eff} as a function of ε_{ee}^R occurs when this parameter cancels the Standard Model right-handed coupling, i.e., at $\varepsilon_{ee}^R = -g_R = -\sin^2 \theta_W$. The same reasoning holds for $\varepsilon_{\tau\tau}^R$, whose minimum appears at the same value.

¹https://bitbucket.org/ahep_cosmo/fortepiano_public

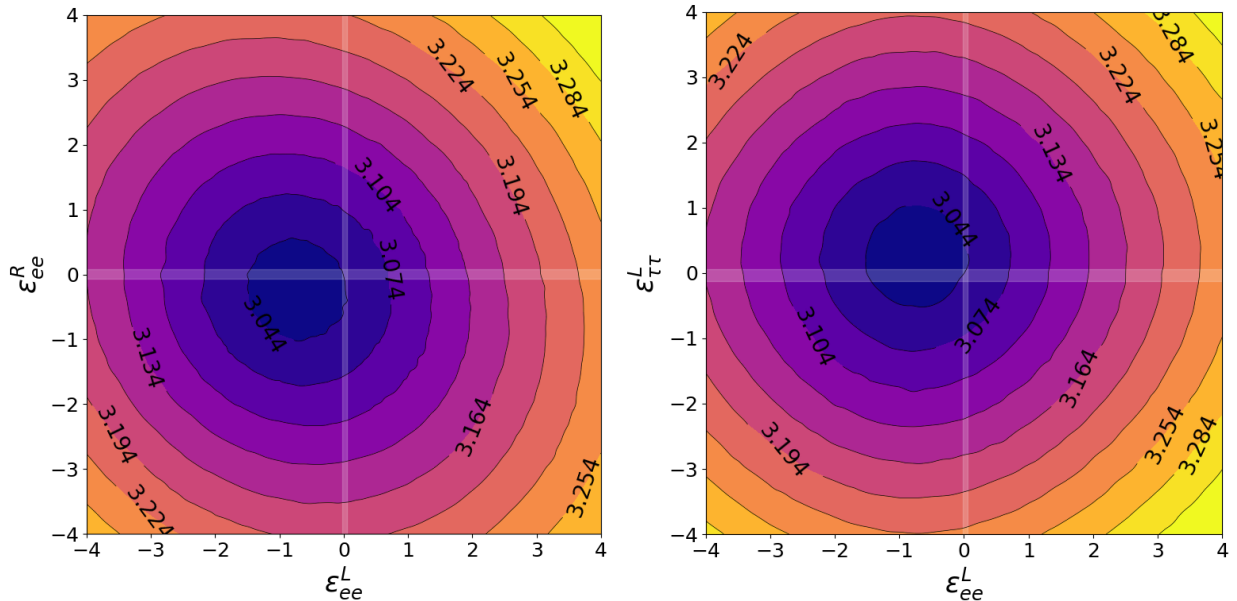


Figure 2: Values of N_{eff} as a function of two diagonal NSI parameters. Left panel: $\epsilon_{ee}^L - \epsilon_{ee}^R$; right panel: $\epsilon_{ee}^L - \epsilon_{\tau\tau}^L$. White-shaded regions correspond to the 90% C.L. experimental bounds obtained varying one parameter at a time (Table 1).

In order to investigate possible interference and combined effects among different NSI parameters, we allow for the simultaneous variation of two couplings. This multidimensional exploration is useful to identify degeneracies in the NSI parameter space that cannot be captured in one-parameter analyses.

As an illustrative example, Fig. 2 shows contours of constant N_{eff} in the plane spanned by different combinations of diagonal left- and right-handed NSI couplings. The resulting iso- N_{eff} contours take an elliptical shape, as expected from the quadratic dependence of the effective neutrino–electron couplings on the NSI parameters, which also determines the location of the minima.

Additional examples of the impact of non-standard neutrino–electron interactions on N_{eff} , for different choices of NSI parameters, are presented in [12]. In the present work, we limit ourselves to a representative subset, as our main focus is on the implications for Big Bang Nucleosynthesis observables.

4. Impact of relic neutrinos on Big Bang Nucleosynthesis

Following the decoupling of neutrinos and the rapid cooling of the early universe, conditions became suitable for the formation of light nuclei. This period, known as Big Bang Nucleosynthesis or primordial nucleosynthesis, marks a key moment in cosmic history: the genesis of the first elements. Occurring within the first few minutes after the Big Bang, BBN relies entirely on well-established SM physics and provides one of the most robust probes of the early universe. It predicts the primordial abundances of light elements such as deuterium (D or ^2H), helium-3 (^3He), helium-4 (^4He), in remarkable agreement with the values inferred from astrophysical observations, see e.g. [23], and lithium-7 (^7Li), which however does not match the observed value [24]. Hence, BBN plays a crucial role in constraining possible deviations from the standard cosmological scenario and probing new physics beyond the Standard Model.

Roughly one second after the Big Bang, when temperatures had dropped to the order of a few MeV, the particle content of the universe was limited to photons, (anti-)neutrinos, electrons, positrons, and a small population of protons and neutrons, all in thermal equilibrium. Despite their low number density, nucleons play a central role during BBN, as they are the fundamental building blocks of the light nuclei that formed during this period. In particular, the neutron-to-proton ratio is a crucial quantity that determines the final elemental abundances, especially the production of helium-4. This ratio is governed by the following

Table 2: Best-fit values for the primordial abundances of light elements, obtained from a combination of observational data as compiled in the 2025 update of [24]. Uncertainties correspond to the 1σ level.

Y_p	0.245 ± 0.003
${}^2\text{H}/\text{H} \times 10^5$	2.508 ± 0.029
${}^7\text{Li}/\text{H} \times 10^{10}$	$> 1.45 \pm 0.25$

charged-current weak interaction processes:

$$\nu_e + n \longleftrightarrow p + e^-, \quad (15)$$

$$e^+ + n \longleftrightarrow p + \bar{\nu}_e, \quad (16)$$

$$n \longleftrightarrow p + e^- + \bar{\nu}_e. \quad (17)$$

Here, n and p refer to neutrons and protons, respectively. If the rates for these interactions are rapid compared to the Hubble expansion rate, the system remains in chemical equilibrium.

After neutrino decoupling, the weak interaction rates involving neutrons and protons fall below the expansion rate of the universe, and chemical equilibrium can no longer be maintained. At temperatures below $T \sim 0.7$ MeV, the neutron-to-proton density ratio departs from its equilibrium value and freezes out, with a residual decrease due to free neutron decays. This effectively sets the neutron abundance prior to the onset of nucleosynthesis.

After the first few minutes following the Big Bang, the baryonic composition of the universe was effectively established. Approximately 75% of the baryonic mass remained in the form of hydrogen nuclei (protons), while nearly 25% became bound in helium-4 nuclei. In addition to these dominant components, trace amounts of other light elements were also present, including deuterium, helium-3, and lithium-7. The observationally inferred values of the primordial abundances, obtained from different astrophysical environments, are summarised in Table 2. These values represent the current best estimates based on high-precision measurements and serve as crucial benchmarks for theoretical predictions from BBN computations. Following the common convention adopted in cosmology, the abundances are given as the mass fraction $Y_p \equiv 4n_{{}^4\text{He}}/n_B$ for helium-4, and the number densities normalised to hydrogen for the other light elements: D/H , ${}^3\text{He}/\text{H}$, and ${}^7\text{Li}/\text{H}$ for deuterium, helium-3, and lithium-7, respectively, where $\text{H} \equiv n_H$, $\text{D} \equiv n_{{}^2\text{H}}$, etc.

In the framework of standard BBN, the theoretical predictions for the primordial abundances of light elements depend on well-established physics and inputs — such as the neutron lifetime and the relevant nuclear reaction rates — and there is only one free cosmological parameter: the baryon-to-photon ratio $\eta_B \equiv n_B/n_\gamma$. This parameter controls the density of baryons available to form nuclei during BBN, and thereby influences the freeze-out and efficiency of the various nuclear reactions. It is often convenient to express it as $\eta_{10} \equiv 10^{10}\eta_B$.

As BBN occurred right after neutrino decoupling, any modification in the decoupling process of relic neutrinos can alter the primordial abundances of light elements. On the one hand, neutrinos contribute to the total radiation energy density, which determines the expansion rate of the universe during the BBN epoch. The effect of all relativistic species beyond photons is parametrised by N_{eff} . Therefore, any deviation from the standard value of this parameter alters the expansion rate and, consequently, the thermal history of the early universe — a mechanism commonly referred to as the *background effect*. This change shifts the timing of the freeze-out of the weak interactions that interconvert neutrons and protons, thereby impacting the neutron-to-proton ratio and the final synthesis of light nuclei. In particular, a larger value of N_{eff} leads to a faster expansion, which causes an earlier n_n/n_p freeze-out. This results in a higher relic abundance of neutrons and ultimately enhances the production of ${}^4\text{He}$ and, to a lesser extent, of D.

On the other hand, electron (anti-)neutrinos participate directly in the charged-current weak interactions that govern the neutron-to-proton chemical equilibrium. Therefore, any deviation from the standard Fermi–Dirac spectra of neutrinos can modify the rates of these weak processes, altering the evolution of the neutron-to-proton ratio. Since this ratio sets the initial conditions for the synthesis of light elements,

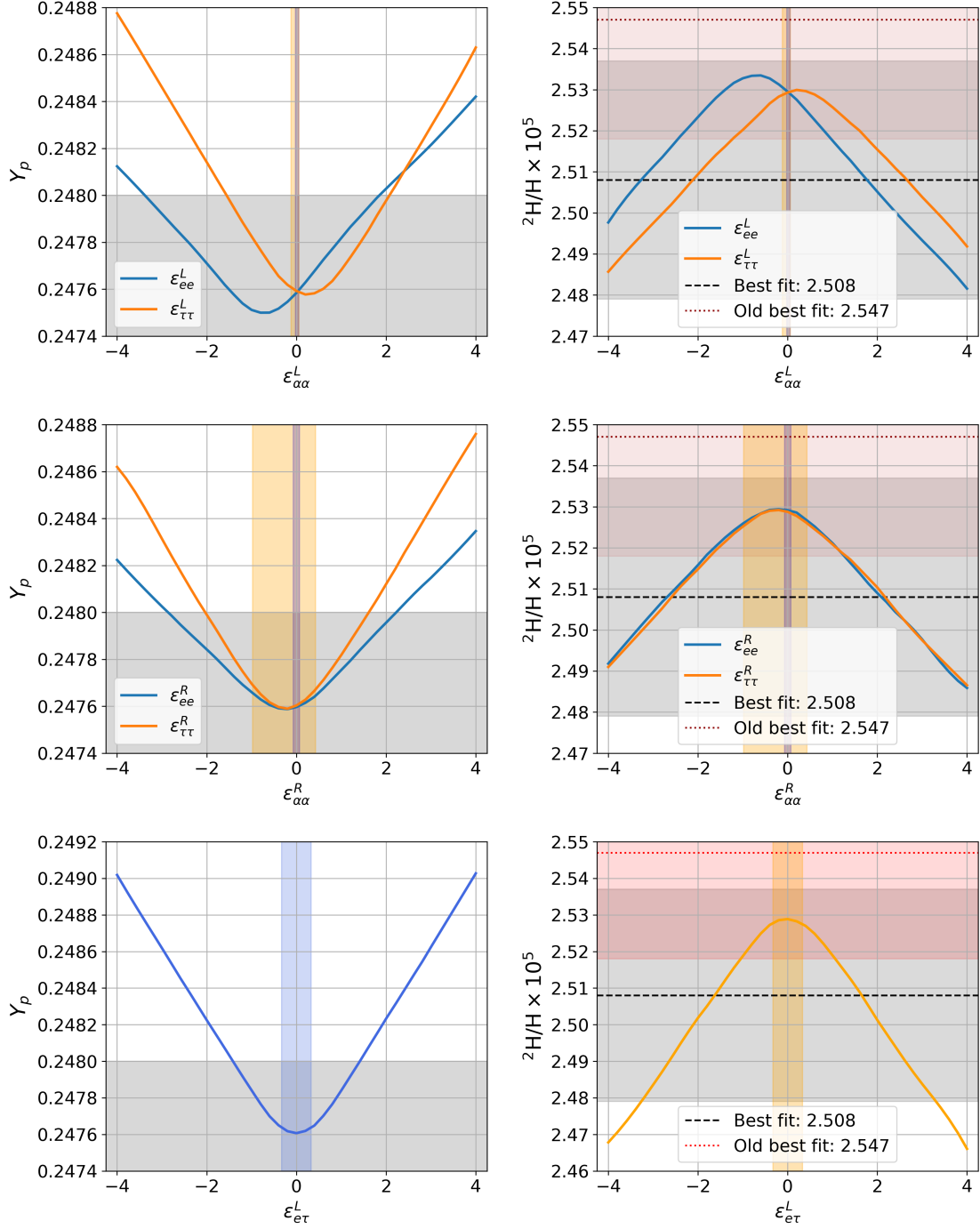


Figure 3: Primordial abundances of helium-4 (mass fraction) and deuterium (number density normalised to hydrogen) as functions of the NSI parameters: non-universal left-handed ϵ_{ee}^L and $\epsilon_{\tau\tau}^L$ (top panel), non-universal right-handed ϵ_{ee}^R and $\epsilon_{\tau\tau}^R$ (middle panel), and left-handed flavour-changing coupling $\epsilon_{e\tau}^L$ (bottom panel). The shaded grey regions correspond to the observational best fit 1σ bounds (Table 2). The shaded red region in the right panel corresponds to the old (2024) recommended observation 1σ bounds for deuterium, see the main text for details. The shaded vertical bands correspond to the 90% C.L. bounds shown in Table 1.

such distortions in the neutrino momentum distributions can lead to measurable changes in the primordial helium-4 mass fraction, as well as in the abundances of other light nuclei.

In order to translate these physical effects into bounds on NSI parameters, a fully numerical treatment of both neutrino decoupling and nuclear reaction networks is required. In this work, we adopt a two-step approach. First, we use the code `FortEPiANO` to compute the evolution of the neutrino momentum distributions throughout the decoupling epoch for different values of the NSI parameters. These time-dependent distributions consistently capture the impact of non-standard interactions on both neutrino spectra and weak interaction rates. The resulting neutrino distributions are then introduced into a modified version of the numerical code `PArthENoPE`² [25, 26, 27], which allows us to compute the corresponding primordial light-element abundances.

By varying only one NSI parameter at a time, we generate predictions for Y_p and ${}^2\text{H}/\text{H}$. The resulting curves are shown in Figure 3. The corresponding results for the right-handed flavour-changing coupling $\varepsilon_{e\tau}^R$ are not shown, as they are qualitatively analogous to those obtained for $\varepsilon_{e\tau}^L$. For the computations, we have assumed $\eta_{10} = 6.12$ (best fit from Planck [7, 24]). These results illustrate how precise measurements of the light-element abundances should be used to constrain NSI parameters, providing a complementary probe to other neutrino observables.

As we can see, the behaviour of the helium mass fraction Y_p closely resembles the trend observed for N_{eff} in Fig. 1. In particular, for non-universal NSI — such as $\varepsilon_{ee}^{L,R}$ and $\varepsilon_{\tau\tau}^{L,R}$ — the minima of Y_p are found around the same values that minimised N_{eff} : approximately $\varepsilon_{ee}^L = -\tilde{g}_L$ for the left-handed electron sector, $\varepsilon_{\tau\tau}^L = -g_L$ for the tau sector, and $\varepsilon_{ee}^R = \varepsilon_{\tau\tau}^R = -g_R$ for right-handed couplings. This behaviour arises from the fact that both Y_p and N_{eff} are sensitive to the modifications in the neutrino momentum spectra and weak interaction rates induced by these couplings.

In the case of the flavour-changing NSI — namely $\varepsilon_{e\tau}^L$ — the helium and deuterium abundances show symmetric behaviour with respect to $\varepsilon_{e\tau}^L = 0$, displaying a clear minimum for Y_p and a maximum for ${}^2\text{H}/\text{H}$ at the origin. This pattern reflects the dependence of the rates on these off-diagonal parameters, which enter in the collision integrals quadratically (see Eqs. (10)–(12)). Consequently, the helium mass fraction increases symmetrically as the magnitude of the flavour-changing parameter grows.

The observed similarity between the behaviours of Y_p and N_{eff} as functions of the NSI parameters is expected. As discussed earlier, an increase in N_{eff} leads to a faster expansion rate of the universe during BBN, which results in a higher relic neutron abundance and consequently an enhanced production of ${}^4\text{He}$.

Nonetheless, there is also a subdominant contribution from the direct modification of the weak interaction rates that govern neutron-proton interconversion. As shown in the first set of reactions in Eqs. (15)–(17), neutrinos participate in the key processes that determine the n_n/n_p ratio. Therefore, changes in the neutrino spectra induced by NSI can slightly alter the balance between these reactions. However, this effect is relatively minor, as evidenced by the fact that no significant deviations from the general trend driven by N_{eff} are observed in the computed abundances. An exception to this pattern appears for sufficiently large absolute values of the electron NSI couplings $\varepsilon_{ee}^{L,R}$, where small but visible departures from the pure N_{eff} -driven trend appear (see Fig. 1). This suggests that in this regime the impact of NSI on the weak interaction rates becomes more pronounced, slightly reducing the neutron abundance available for helium synthesis despite the increase in the expansion rate.

The behaviour of the deuterium abundance differs from that of the helium mass fraction and requires a more careful interpretation. In the presence of non-standard neutrino interactions, neutrinos remain coupled to the electromagnetic plasma for a longer time with respect to the standard e^+e^- annihilation epoch. This prolonged coupling modifies the time–temperature relation during the phase in which nuclear reactions are active, affecting the efficiency of deuterium burning.

If only the effect of an increased radiation density and a faster expansion rate were taken into account, one would expect a larger final deuterium abundance, since the reduced available time would hinder deuterium destruction (see e.g. [6]). However, the dominant effect induced by NSI is instead associated with the modified thermal history of the plasma, which leads to a more efficient processing of deuterium into heavier nuclei. As a consequence, the final ${}^2\text{H}/\text{H}$ abundance is reduced with respect to the standard case.

²<https://parthenope.na.infn.it/>

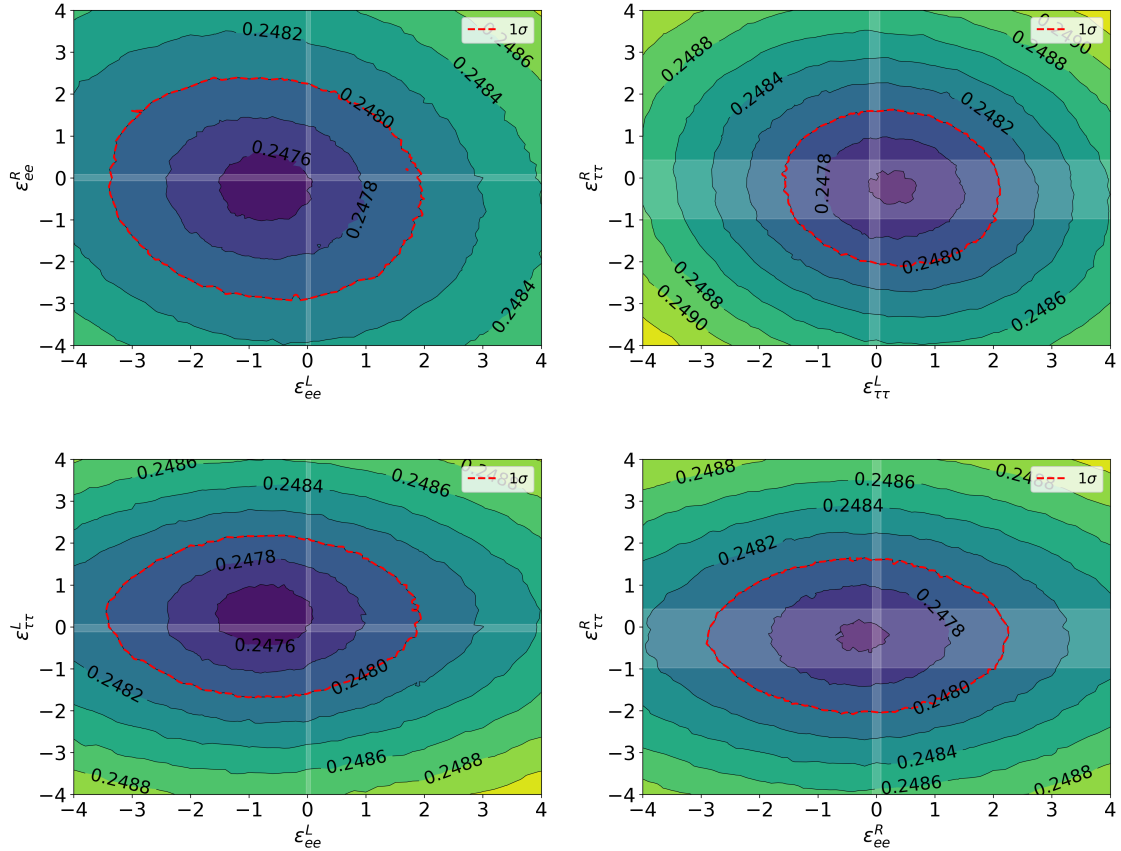


Figure 4: Values of Y_p when varying two diagonal NSI parameters simultaneously. Top left panel: $\varepsilon_{ee}^L - \varepsilon_{ee}^R$; top right panel: $\varepsilon_{\tau\tau}^L - \varepsilon_{\tau\tau}^R$; bottom left panel: $\varepsilon_{ee}^L - \varepsilon_{\tau\tau}^L$; bottom right panel: $\varepsilon_{ee}^R - \varepsilon_{\tau\tau}^R$. White-shaded regions correspond to the 90% C.L. experimental bounds obtained varying one parameter at a time (Table 1). The dashed red curve corresponds to the observational 1σ bound (Table 2).

The observationally allowed regions for both Y_p and ${}^2\text{H}/\text{H}$ are marked in the plots as shaded bands, corresponding to $Y_p = 0.245 \pm 0.003$ and ${}^2\text{H}/\text{H} = (2.508 \pm 0.029) \times 10^{-5}$. These bands allow us to extract approximate 1σ constraints for each NSI parameter. Although these cosmological bounds are significantly weaker than current laboratory limits (see Table 1), they provide a complementary probe that is sensitive to physics at the time of neutrino decoupling.

In the case of deuterium, we additionally indicate the previous observational 1σ interval used at earlier stages of this project, ${}^2\text{H}/\text{H} = (2.547 \pm 0.029) \times 10^{-5}$, taken from [24] before the 2025 update. The comparison highlights how updates in the inferred primordial deuterium abundance directly translate into changes in the strength of the resulting cosmological constraints.

The conclusions drawn from the one-dimensional analysis are further supported by the two-dimensional scans. In the Y_p contours shown in Fig. 4, the dependence on pairs of NSI parameters closely follows the behaviour expected from the corresponding variations in N_{eff} , reflecting the dominant role of the expansion rate in determining the helium abundance. Conversely, the deuterium abundance exhibits the opposite trend, as illustrated in Fig. 5, with regions of parameter space associated with larger values of N_{eff} typically leading to lower ${}^2\text{H}/\text{H}$ abundances. This behaviour is also evident in the off-diagonal cases, such as the example shown in Fig. 6, where a symmetric structure around the minimum of Y_p corresponds to a maximum in the deuterium abundance.

Overall, the two-dimensional results provide a consistent visual confirmation of the physical picture

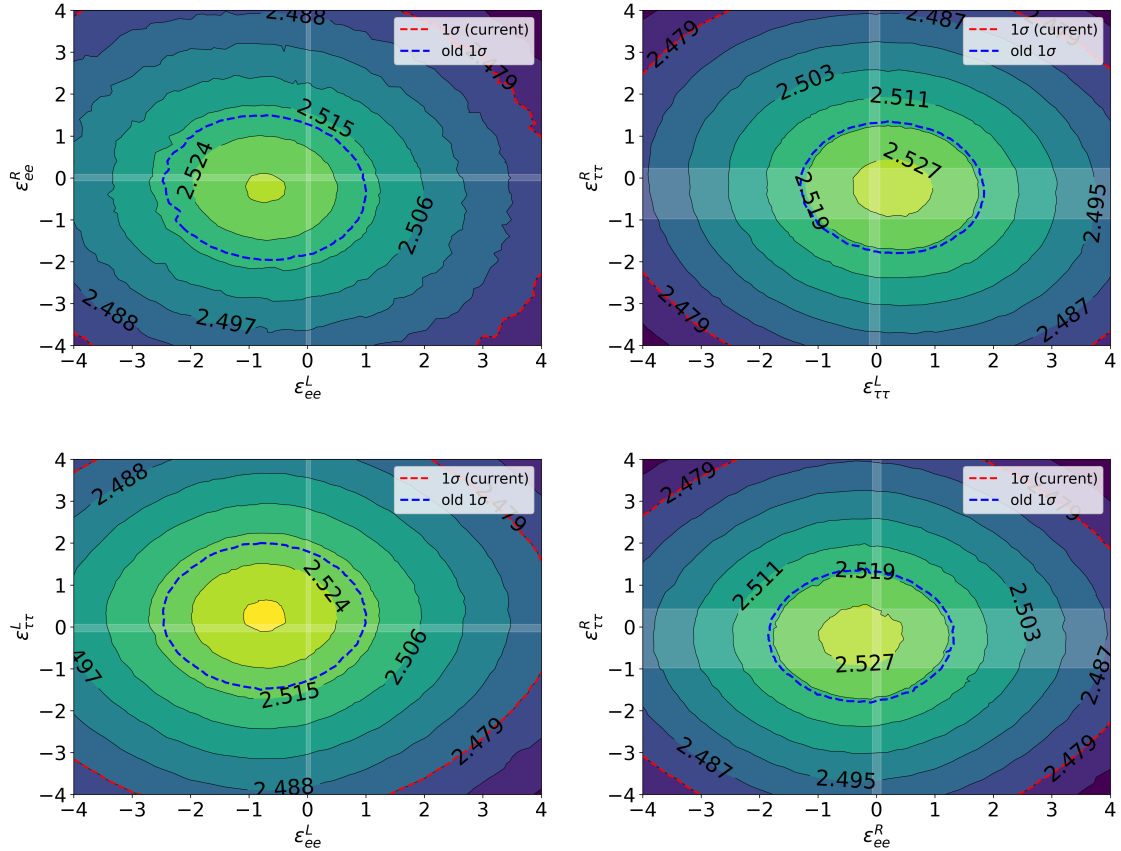


Figure 5: Same as Fig. 4, but for ${}^2\text{H}/\text{H}$ abundances. The dashed blue curve corresponds to the 1σ bound based on the old (2024) best fit for deuterium.

emerging from the one-dimensional analysis: while Y_p largely tracks the background expansion history, the deuterium abundance remains more sensitive to the detailed thermal evolution during the nucleosynthesis epoch.

5. Conclusions

In this work, we have explored some of the cosmological implications of neutrino non-standard interactions with electrons, focusing on their impact during two key stages in the early universe: neutrino decoupling and Big Bang Nucleosynthesis. These epochs are particularly sensitive to the properties of neutrinos and thus offer a unique opportunity to probe possible deviations from Standard Model predictions.

As a first step, we studied the effect of non-standard interactions on neutrino decoupling, reproducing the results obtained in Ref. [12] for the effective number of relativistic species N_{eff} . We extended this analysis by exploring a wider region of the NSI parameter space, confirming the robustness of the numerical framework and using N_{eff} as a diagnostic quantity to characterise the impact of NSI on the thermal history of the early universe.

For the first time, we have calculated the impact of neutrino NSI with electrons on Big Bang Nucleosynthesis, focusing on the primordial helium mass fraction Y_p and the deuterium-to-hydrogen ratio ${}^2\text{H}/\text{H}$. Our results show that the behaviour of Y_p closely tracks that of N_{eff} , reflecting the dominant role of the expansion rate in determining the helium abundance. Subdominant effects arising from direct modifications of the weak interaction rates become relevant only in specific regions of the parameter space.

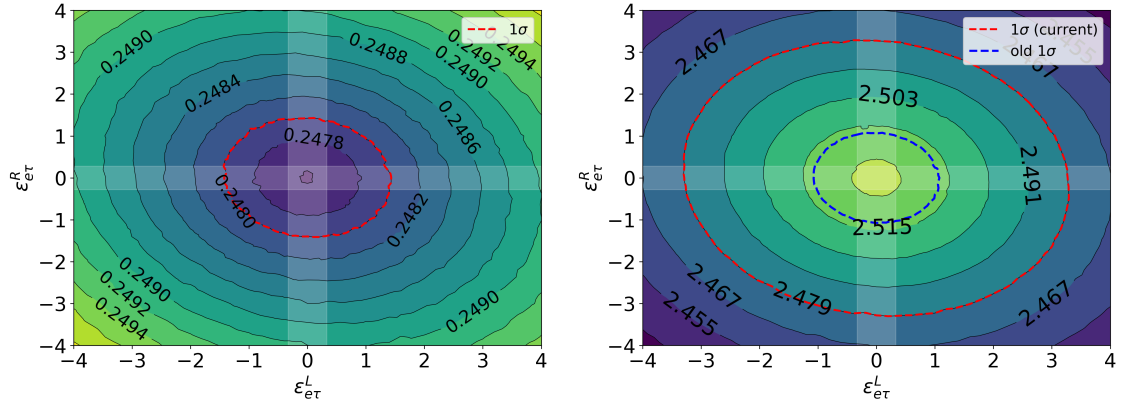


Figure 6: Values of Y_p (left panel) and ${}^2\text{H}/\text{H}$ (right panel) for the simultaneous variation of the flavour-changing NSI parameters $\epsilon_{e\tau}^L$ and $\epsilon_{e\tau}^R$. White-shaded regions correspond to the 90% C.L. experimental bounds obtained varying one parameter at a time (Table 1). The dashed red curve corresponds to the observational 1σ bound (Table 2). The dashed blue curve (right panel) corresponds to the 1σ bound based on the old (2024) best fit for deuterium.

In contrast, the deuterium abundance exhibits a different dependence on non-standard interactions. We find that it is particularly affected by the modified thermal evolution induced by prolonged neutrino–plasma coupling, making ${}^2\text{H}/\text{H}$ a complementary probe of non-standard neutrino interactions during BBN.

Although a large part of the NSI parameter space explored in this work is already constrained by terrestrial experiments, the extended ranges considered here were deliberately chosen to characterise the response of neutrino decoupling and BBN observables to non-standard interactions. The resulting cosmological bounds should therefore be interpreted as complementary to laboratory constraints, probing neutrino properties at vastly different energy and time scales.

Finally, we note that the cosmological constraints derived from Big Bang Nucleosynthesis depend on the adopted determination of the primordial deuterium abundances. Earlier measurements [24], such as those used at the initial stages of this project, led to more restrictive allowed regions in NSI parameter space, while the updated deuterium determination reported by the Particle Data Group results in comparatively weaker constraints. Future improvements in the precision of primordial abundance measurements, particularly for deuterium and helium, could further enhance the sensitivity of cosmological probes to non-standard neutrino interactions. In this context, cosmology will continue to play a vital role in unveiling the fundamental properties of neutrinos and in testing new physics beyond the Standard Model.

Acknowledgments

At IFIC Valencia, this work was supported by the Spanish grants PID2023-147306NB-I00 and CEX2023-001292-S (MCIU/AEI/10.13039/501100011033). J.M. is supported by the grant FPU24/00735. S.G. also acknowledges financial support through the Ramón y Cajal contract RYC2023-044611-I funded by MCIU/AEI/10.13039/501100011033 and FSE+. S.G. and O.P. are supported by the Research grant TAsP (Theoretical Astroparticle Physics) funded by Istituto Nazionale di Fisica Nucleare (INFN). O.P. is also supported by Ministero dell’Università e della Ricerca (MUR), PRIN2022 program (Grant PANTHEON 2022E2J4RK) Italy.

References

- [1] P. F. de Salas, et al., 2020 Global reassessment of the neutrino oscillation picture, JHEP 02 (2021) 071. arXiv:2006.11237, doi:10.1007/JHEP02(2021)071.

- [2] Y. Farzan, M. Tórtola, Neutrino oscillations and Non-Standard Interactions, *Front. in Phys.* 6 (2018) 10. [arXiv:1710.09360](#), [doi:10.3389/fphy.2018.00010](#).
- [3] K. Akita, M. Yamaguchi, A precision calculation of relic neutrino decoupling, *JCAP* 08 (2020) 012. [arXiv:2005.07047](#), [doi:10.1088/1475-7516/2020/08/012](#).
- [4] J. Froustey, C. Pitrou, M. C. Volpe, Neutrino decoupling including flavour oscillations and primordial nucleosynthesis, *JCAP* 12 (2020) 015. [arXiv:2008.01074](#), [doi:10.1088/1475-7516/2020/12/015](#).
- [5] J. J. Bennett, G. Buldgen, P. F. De Salas, M. Drewes, S. Gariazzo, S. Pastor, Y. Y. Y. Wong, Towards a precision calculation of N_{eff} in the Standard Model II: Neutrino decoupling in the presence of flavour oscillations and finite-temperature QED, *JCAP* 04 (2021) 073. [arXiv:2012.02726](#), [doi:10.1007/JCAP04\(2021\)073](#).
- [6] J. Lesgourgues, G. Mangano, G. Miele, S. Pastor, *Neutrino Cosmology*, Cambridge University Press, 2013. [doi:10.1017/CB09781139012874](#).
- [7] N. Aghanim, et al., Planck 2018 results. VI. Cosmological parameters, *Astron. Astrophys.* 641 (2020) A6. [arXiv:1807.06209](#), [doi:10.1051/0004-6361/201833910](#).
- [8] Z. Berezhiani, A. Rossi, Limits on the nonstandard interactions of neutrinos from e^+e^- colliders, *Phys. Lett. B* 535 (2002) 207–218. [arXiv:hep-ph/0111137](#), [doi:10.1016/S0370-2693\(02\)01767-7](#).
- [9] S. Davidson, C. Peña Garay, N. Rius, A. Santamaria, Present and future bounds on nonstandard neutrino interactions, *JHEP* 03 (2003) 011. [arXiv:hep-ph/0302093](#), [doi:10.1088/1126-6708/2003/03/011](#).
- [10] G. Mangano, G. Miele, S. Pastor, T. Pinto, O. Pisanti, P. D. Serpico, Effects of non-standard neutrino-electron interactions on relic neutrino decoupling, *Nucl. Phys. B* 756 (2006) 100–116. [arXiv:hep-ph/0607267](#), [doi:10.1016/j.nuclphysb.2006.09.002](#).
- [11] P. F. de Salas, S. Pastor, Relic neutrino decoupling with flavour oscillations revisited, *JCAP* 07 (2016) 051. [arXiv:1606.06986](#), [doi:10.1088/1475-7516/2016/07/051](#).
- [12] P. F. de Salas, S. Gariazzo, P. Martínez-Miravé, S. Pastor, M. Tórtola, Cosmological radiation density with non-standard neutrino-electron interactions, *Phys. Lett. B* 820 (2021) 136508. [arXiv:2105.08168](#), [doi:10.1016/j.physletb.2021.136508](#).
- [13] G. Barenboim, S. Gariazzo, A. Sánchez-Vargas, Big Bang Nucleosynthesis as a probe of non-standard neutrino interactions and non-unitary three-neutrino mixing, *JCAP* 08 (2025) 005. [arXiv:2503.21998](#), [doi:10.1088/1475-7516/2025/08/005](#).
- [14] P. Coloma, M. C. Gonzalez-Garcia, M. Maltoni, J. P. Pinheiro, S. Urrea, Global constraints on non-standard neutrino interactions with quarks and electrons, *JHEP* 08 (2023) 032. [arXiv:2305.07698](#), [doi:10.1007/JHEP08\(2023\)032](#).
- [15] P. Martínez-Miravé, Neutrino properties from the laboratory and the cosmos, Ph.D. thesis, Valencia U. (2023). [arXiv:2309.15446](#).
- [16] A. Bolaños, O. G. Miranda, A. Palazzo, M. A. Tórtola, J. W. F. Valle, Probing non-standard neutrino-electron interactions with solar and reactor neutrinos, *Phys. Rev. D* 79 (2009) 113012. [arXiv:0812.4417](#), [doi:10.1103/PhysRevD.79.113012](#).
- [17] M. Deniz, et al., Constraints on Non-Standard Neutrino Interactions and Unparticle Physics with Neutrino-Electron Scattering at the Kuo-Sheng Nuclear Power Reactor, *Phys. Rev. D* 82 (2010) 033004. [arXiv:1006.1947](#), [doi:10.1103/PhysRevD.82.033004](#).

- [18] P. Coloma, M. C. Gonzalez-Garcia, M. Maltoni, J. P. Pinheiro, S. Urrea, Constraining new physics with Borexino Phase-II spectral data, *JHEP* 07 (2022) 138, [Erratum: *JHEP* 11 (2022) 138]. [arXiv:2204.03011](#), [doi:10.1007/JHEP07\(2022\)138](#).
- [19] J. Barranco, O. G. Miranda, C. A. Moura, J. W. F. Valle, Constraining non-standard neutrino-electron interactions, *Phys. Rev. D* 77 (2008) 093014. [arXiv:0711.0698](#), [doi:10.1103/PhysRevD.77.093014](#).
- [20] S. K. Agarwalla, F. Lombardi, T. Takeuchi, Constraining Non-Standard Interactions of the Neutrino with Borexino, *JHEP* 12 (2012) 079. [arXiv:1207.3492](#), [doi:10.1007/JHEP12\(2012\)079](#).
- [21] S. Gariazzo, P. F. de Salas, S. Pastor, Thermalisation of sterile neutrinos in the early Universe in the 3+1 scheme with full mixing matrix, *JCAP* 07 (2019) 014. [arXiv:1905.11290](#), [doi:10.1088/1475-7516/2019/07/014](#).
- [22] P. Ade, et al., The Simons Observatory: Science goals and forecasts, *JCAP* 02 (2019) 056. [arXiv:1808.07445](#), [doi:10.1088/1475-7516/2019/02/056](#).
- [23] B. D. Fields, K. A. Olive, T.-H. Yeh, C. Young, Big-Bang Nucleosynthesis after Planck, *JCAP* 03 (2020) 010, [Erratum: *JCAP* 11 (2020) E02]. [arXiv:1912.01132](#), [doi:10.1088/1475-7516/2020/03/010](#).
- [24] S. Navas, et al., Review of particle physics, *Phys. Rev. D* 110 (2024) 030001. [doi:10.1103/PhysRevD.110.030001](#).
- [25] O. Pisanti, A. Cirillo, S. Esposito, F. Iocco, G. Mangano, G. Miele, P. D. Serpico, PArthENoPE: Public Algorithm Evaluating the Nucleosynthesis of Primordial Elements, *Comput. Phys. Commun.* 178 (2008) 956–971. [arXiv:0705.0290](#), [doi:10.1016/j.cpc.2008.02.015](#).
- [26] R. Consiglio, P. F. de Salas, G. Mangano, G. Miele, S. Pastor, O. Pisanti, PArthENoPE reloaded, *Comput. Phys. Commun.* 233 (2018) 237–242. [arXiv:1712.04378](#), [doi:10.1016/j.cpc.2018.06.022](#).
- [27] S. Gariazzo, P. F. de Salas, O. Pisanti, R. Consiglio, PArthENoPE revolutions, *Comput. Phys. Commun.* 271 (2022) 108205. [arXiv:2103.05027](#), [doi:10.1016/j.cpc.2021.108205](#).